Dispersion Polymerization of Methyl Methacrylate in Supercritical Carbon Dioxide Using a Pseudo-Graft Stabilizer: Role of Reactor Mixing

Ana Rosell, Giuseppe Storti, and Massimo Morbidelli*

Swiss Federal Institute of Technology Zurich, Institut für Chemie- und Bioingenieurwissenschaften, ETH−Hönggerberg/HCI, CH-8093 Zürich, Switzerland

Daniel Bratton and Steven M. Howdle

School of Chemistry, University of Nottingham, University Park, Nottingham, NG7 2RD, England

Received May 9, 2003; Revised Manuscript Received February 17, 2004

ABSTRACT: The free radical polymerization of methyl methacrylate (MMA) in supercritical carbon dioxide ($scCO_2$) using a commercially available acid-terminated perfluoropolyether as a stabilizer (Krytox 157 FSL) is analyzed experimentally. A series of polymerizations were carried out under identical conditions; only the rate of stirring was varied. At each specific stirring rate, the complete evolution of conversion and molecular weight was obtained by repeated experiments quenched at different times. The results obtained indicate that the dispersion becomes unstable at a surprisingly moderate stirring rate (above 25 rpm). Clearly, the anchoring interaction of the Krytox stabilizer is relatively weak, and destabilization occurs at modest shear induced by the mechanical stirring. However, when stable conditions are achieved, normal kinetic behavior is observed, leading to a fluffy polymer, with uniform particle size in the range of few microns and relatively broad molecular weight distribution. A particular attraction of these stabilizers is that the anchoring interactions occur via a hydrogen-bonding mechanism which is reversible; thus, no residues of stabilizer are found in the final PMMA product, and the stabilizer is vented with CO_2. Apart from the shift of the high molecular weights, likely due to diffusion limitations in the polymer particles at high conversion, this broad molecular weight distribution is a result of the combined action of two reaction loci: the polymer particles and the continuous phase. Even under stable conditions, although the polymer particles are clearly the dominant locus of polymerization, the contribution of the polymerization in the continuous phase cannot be neglected.

1. Introduction

Polymerization reactions in supercritical CO_2 are being investigated by many research groups, and comprehensive reviews are available (e.g., refs 1 and 2). Monomer−CO_2 mixtures typically exhibit a type I phase behavior (cf. ref 3), meaning that they are miscible in all proportions, and as a consequence, all polymerization processes in $scCO_2$ start homogeneously. However, at practical operating conditions, only amorphous, low melting fluoropolymers and polysiloxanes have been found to be sufficiently soluble in CO_2 to allow a completely homogeneous polymerization, a process which is now considered an alternative to current technologies for these polymers.[4] On the contrary, most of the standard vinyl polymers are practically insoluble in $scCO_2$, and therefore they precipitate out as a second phase while being formed, leading to a heterogeneous process. For semicrystalline polymers, such as poly(acrylic acid)[5] and poly(vinylidene difluoride),[6] a precipitation mechanism is appropriate, and polymerization can be conducted successfully. However, for most other vinyl monomers under these conditions, good yields and molecular weights are achieved only if a dispersant is added to stabilize the precipitating polymer particles and to get the final product as a powder. For this reason, dispersion polymerization appears to be the most effective process to polymerize vinyl monomers in $scCO_2$.

Dispersants (or stabilizers) play a key role in dispersion polymerization (cf. ref 7). For successful polymerization in CO_2 the conventional dispersants are not appropriate, and careful design of efficient stabilizers is an essential step toward the development of competitive technologies based on this kind of polymerization in $scCO_2$. Since CO_2 has a very low dielectric constant, steric stabilization by polymeric stabilizers is the mechanism of choice for carbon dioxide.[1,8] Typically, a steric stabilizer is a macromolecule which is preferentially located at the polymer−solvent interface and prevents aggregation by coating the particle surface and imparting long-range repulsions. Steric stabilizers stick to the surface of the polymer particles by either grafting or physical adsorption. An effective stabilizer should be soluble in CO_2 at operating conditions, while interacting with the polymer in a thermodynamically favorable way. Factors that contribute to increase its solubility in CO_2 are low polarizability, low solubility parameter, and electron donating capability, given that CO_2 is a weak Lewis acid. Fluoroethers, fluoroalkanes, fluoroacrylates, and siloxanes exhibit high compatibility with liquid or supercritical CO_2.[9] Moreover, nonfluorinated polymers, in particular poly(ether−carbonates), have been recently proposed, displaying high solubility in CO_2 even at low pressures.[10]

Among the many alternatives, the commercially available stabilizer Krytox 157 FSL has been proved effective in the dispersion polymerization of methyl methacrylate by Christian et al.[11] This stabilizer ($M_n \sim 2500$ g/mol; structure in Figure 1) is a low molecular weight, monofunctional carboxylic acid-terminated perfluoropolyether. Its mechanism of stabilization is be-

* To whom correspondence should be addressed.

10.1021/ma030262w CCC: $27.50
Published on Web 03/26/2004

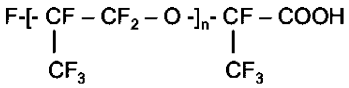

Figure 1. Structure of Krytox 157 FSL ($n \sim 14$).

lieved to be based on the formation of a relatively weak hydrogen bond between the terminal acid functionality of the stabilizer and the ester groups of poly-MMA. Therefore, its behavior resembles that of grafting stabilizers, thus justifying its definition of "pseudo-graft" stabilizer.[11] On one hand, the main advantage of this weak interaction is its reversibility, such that no residual stabilizer is usually detected in the final polymer after depressurization.[12] On the other hand, this leads to a weak stabilization which could pose limitations in terms of reactor operating conditions and, specifically, of mixing rate.

Operational difficulties related to reactor mixing have been previously reported in the literature. For the dispersion polymerization of poly-MMA but a different stabilizer (PDMS-mMA), Christian et al.[13] reported that both polymer yield and molecular weights were strongly affected by mixing. Surprisingly, improved yields and molecular weights were obtained in the *absence* of stirring. The authors concluded that some kind of termination reaction was occurring between the propagating radicals and the steel walls of the autoclave. However, in the absence of stirring, a high molecular weight poly-MMA film was deposited on the walls, thus preventing this termination reaction. It was suggested that the deposition of this passivating film was hindered by efficient agitation and that this additional termination is the reason for the low monomer conversion and molecular weight under stirring. Most of the reported literature on dispersion polymerization cites experiments carried out in autoclaves and view cells using magnetically coupled "flea" type stirrer bars in which the level of shear induced is likely to be very low. In addition as the reaction proceeds, the level of polymer solids in the vessel in the reaction solution begins to increase, and it is unlikely that stirring continues for any significant period of time. Moreover, the stirrer itself is often not visible after the first few minutes of polymerization reaction.

This work reports the results of an experimental analysis of the dispersion polymerization of methyl methacrylate in supercritical CO_2 using Krytox 157 FSL as stabilizer. The aim is to deepen the understanding of the behavior of the process carried out in a mechanically stirred reactor with this specific kind of "weak" stabilizer. Kinetic experiments were performed in a lab-scale setup, designed and built with special attention to the accurate measurement of the amount of CO_2 fed to the reactor. To investigate the effect of stirring speed on reaction kinetics, experiments at different stirring speeds were performed. As soon as stable conditions were identified, the evolution of conversion and polymer properties with time was obtained by repeated reactions with the same recipe but stopped at different times. Combining particle morphology and molecular weight characterizations, an explanation of the system behavior under stirring is given.

2. Materials and Methods

2.1. Materials. Methyl methacrylate, 2,2′-azobis(isobutyronitrile) (AIBN), tetrahydrofuran (THF), methylene chloride, methanol, and hydroquinone were obtained from Fluka (Switzerland) and used as received. Carbon dioxide was obtained by Pangas (Switzerland) with analytic grade 4.0 (purity = 99.99%) and used as received. Krytox 157 FSL was kindly supplied by Dupont (Switzerland) and used as received.

2.2. Experimental Setup. Experiments were carried out in the lab-scale unit sketched in Figure 2. The unit was designed to run batch polymerization reactions at high pressure, with accurate evaluation of the amount of CO_2 fed to the reactor. The accuracy of this measurement is of major importance not only for experimental reproducibility but also for subsequent modeling analysis. The unit can be divided into three modules: the reactor, the CO_2 feeding system, and the CO_2 purge line. The reactor (a stainless steel double-jacketed autoclave, model HPM-P by PREMEX (Switzerland), nominal internal volume of 500 mL, maximum operating temperature and pressure of 200 °C and 200 bar, respectively) is equipped with a magnetically coupled mechanical stirrer, with maximum stirring speed of 1000 rpm. Three different impeller types were used: a stainless steel impeller with gas

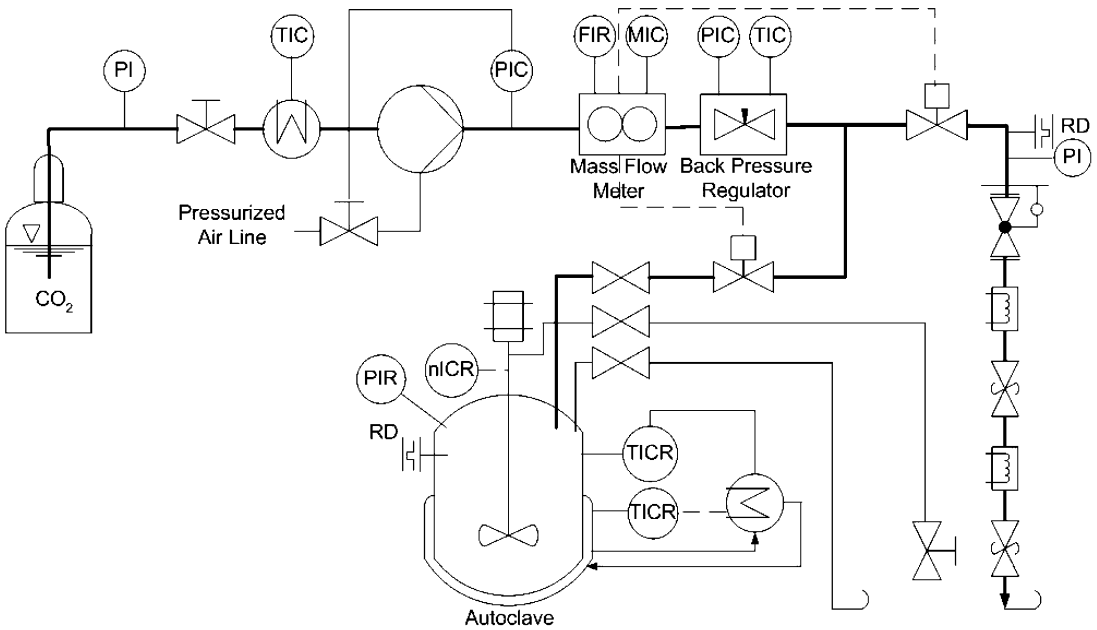

Figure 2. Scheme of the polymerization unit. RD = rupture disk; XI = indicator; XIR = indicator and recorder; XIC = indicator and controller; XICR = indicator, controller, and recorder.

Table 1. Dispersion Polymerization of MMA in Supercritical CO_2 (Stabilizer: Krytox 157 FSL; Initiator: AIBN); Polymerization Conditions and Product Characteristics

run	stirring rate (rpm)	time (h)	final pressure (bar)	final conversion	M_w (kg/mol)	P_d	product remarks
1a	25	1.15	130	0.28	123.8	3.2	oil/tacky solid
1b	25	1.55	140	0.50	180.4	3.5	tacky solid
1c	25	1.70	150	0.63	222.6	4.3	tacky solid/coagulated powder
1d	25	1.85	160	0.72	344.4	3.9	uncoagulated powder
1e	25	2.90	170	0.98	450.9	4.6	uncoagulated fluffy powder
2[a]	25	3.00	130	0.20	20.7	2.2	oil
3	0	3.00	165	high	406.7	3.9	uncoagulated fluffy powder
4	15	3.00	166	high	405.2	2.3	uncoagulated fluffy powder
5	45	3.00	169	high	417.1	3.5	tacky solid/coagulated powder
6	100	3.00	150	medium	263.9	4.5	oil/coagulated solid
7	400	3.00	130	low	23.3	2.2	oil

[a] Experimental run without stabilizer.

sparger facility and two standard turbines made of stainless steel and Ti. All of them were designed with four equally spaced, vertical blades. The CO_2 feeding line includes a high-pressure piston pump for liquid CO_2 (NWA GmbH, Germany) followed by a pulse dampener, a mass flowmeter (RHM 015 GNT by Rheonik, Germany) with mass counter integrator, and an automatic back-pressure regulator (BPRA-200 by Thar Designs). The mass flowmeter, based on Coriolis force, provides two electronic outputs which are used to control two magnetic valves located on the venting line and the reactor feed line, respectively. The back-pressure regulator is made of an automatic needle valve housed in a thermostatic chamber. This is an important feature since mild pressure drops are sufficient to freeze the CO_2 inside the valve. Through this regulator, constant back-pressure is achieved which ensures the correct operation of the flow meter. The venting line is constituted by a series of valves and heat exchangers to depressurize the CO_2 in a multistep expansion procedure, so as to avoid freezing in and clogging of the line. The valve pressure drops have been adjusted to distribute the overall pressure drop as uniformly as possible. The actual reactor volume was determined by loading the vessel with a known amount of carbon dioxide and measuring the resulting pressure after temperature equilibration. Using tabulated values of the thermodynamic properties of pure carbon dioxide,[14] the corresponding density was determined and the reactor volume estimated. From repeated experiments at different conditions of injected amount and temperature, the actual reactor volume was estimated as 566 ± 4 mL.

2.3. Reaction Procedure. Given amounts of monomer, stabilizer, and initiator are directly charged to the reactor at room temperature. The reactor is sealed and stirring started. Carbon dioxide is initially pumped through the venting line and a constant mass flow rate of about 30 g/min is achieved in few minutes. Then, the magnetic valve of the venting line is closed while automatically opening the magnetic valve of the feed line. At the same time, the batch mass counter of the flowmeter starts, and the reactor is filled with CO_2 at practically constant flow. Once the desired amount of CO_2 has been charged, the magnetic valve closes automatically. The set point of the reactor temperature is then raised to the desired operating temperature, which is achieved in approximately 1 h. Experiments have been performed by adding the initiator after reactor thermal equilibration to confirm that no polymerization occurs during this heating time. This is mainly due to the presence of significant induction times in all experiments, which are long enough to ensure that no polymerization takes place before thermal equilibration is achieved. The reaction is typically run for 4 h, and for kinetic investigation, several reactions with the same recipe are repeated and quenched at different times. To quench the reaction, stirring is stopped; the reactor is then rapidly cooled to room temperature and slowly depressurized through the purge line. Depressurization is slow (about half an hour) to prevent freezing of CO_2. Then, the reactor is opened, and samples are taken for further characterizations. Finally, the reactor is mechanically cleaned with sand at high pressure if dispersion instability resulted in polymer fouling. In all cases it was washed with solvents (THF and methylene chloride) and flushed with CO_2 before each experiment.

2.4. Polymer Characterizations. To evaluate conversion, most of the polymer was recovered by hand with a spatula while the rest was dissolved in a solution of tetrahydrofuran and hydroquinone and precipitated in an excess of methanol. Then, the overall polymer was dried for several hours at 80 °C to remove residual monomer and solvents, and conversion was determined gravimetrically. Since the accurate recovery of the whole amount of produced polymer can be very difficult (in particular when polymer coagulation occurs), the final conversion measurements were carried out only for the reactions at stirring speed of 25 rpm.

Two different procedures have been applied to samples for particle and molecular weight characterization. For particle morphology, the sample as taken from the reactor was placed under vacuum at room temperature for several hours. For molecular weight analysis, the sample was dissolved in a solution of methanol and hydroquinone and again placed under vacuum at room temperature for several hours. Particle morphology and average size were analyzed by scanning electron microscopy (SEM). Gel permeation chromatography (GPC) (Hewlett-Packard, series 1100) was used to determine the complete distribution of molecular weight, MWD. The instrument is equipped with three columns (Polymer Standards, UK, Plgel 5μ, Mixed C) and refractive index detector. Tetrahydrofuran was used as eluent at a flow rate of 1 mL/min and temperature of 25 °C. The molecular weight vs elution time calibration curve was determined using seven monodispersed polystyrene standards (Polymer Standards, UK), covering a range of molecular weight from 5.0×10^3 to 1.29×10^6 g/mol. The Mark−Houwink equation was used to evaluate the calibration curve of poly-MMA from the calibration curve of polystyrene.

3. Results

All reactions detailed in Table 1 were performed with the following recipe unless differently specified: MMA = 90 g, CO_2 = 320 g, AIBN = 1 g, Krytox 157 FSL = 1 g, and temperature = 65 °C.

Let us examine first the experiments at different stirring speeds, namely 0, 15, 25, 45, 100, and 400 rpm (entries 1e and 3−7 in Table 1). Figure 3 shows the experimental pressure−time evolutions. The pressure profile displays a sharp increase in time for stirring speeds lower than 45 rpm. At higher speeds the slope is significantly reduced, and at the maximum considered stirring rate (entry 7, 400 rpm), pressure remains practically constant for the entire experiment. An equivalent behavior was observed in terms of final conversion: practically complete for all the experiments at stirring speed lower than 45 rpm but significantly smaller at 100 and 400 rpm. Therefore, a clear interplay

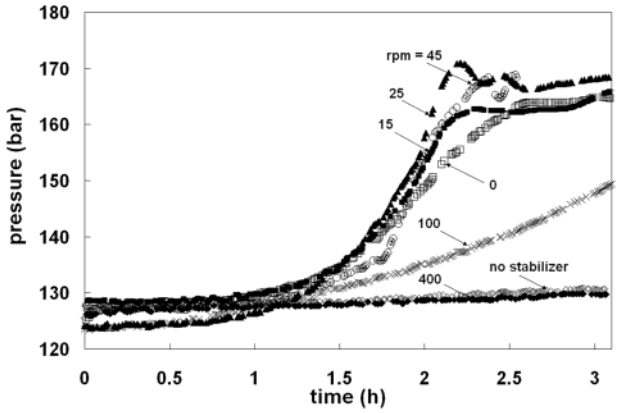

Figure 3. Pressure vs time evolution at different stirring speeds. Numerical labels correspond to stirring speed in rpm (runs 1e and 3 to 7 in Table 1); the label "no stabilizer" corresponds to run 2 in Table 1.

between reaction and stirring rate was identified at stirring rates above 45 rpm. It is important to note that, above 400 rpm, the reaction rate becomes practically equal to that observed at low stirring speed (25 rpm) but without stabilizer (entry 2 in Table 1).

Also, polymer morphology changes significantly with stirring speed. From a macroscopic point of view, the final products display an increasing extent of coagulation at increasing stirring speed, as summarized in the last column of Table 1. The SEM pictures shown in Figure 4 confirm this observation. Namely, the images obtained for runs 3 and 1e (at 0 and 25 rpm, respectively) show rather monodisperse, segregated polymer particles in the micron size. The presence of a pearl necklace microstructure is evident for run 1e, indicating that the final particles are not completely separated but somehow slightly aggregated already at very low stirring speed. Similar microstructures have been reported by Christian et al.[12] using the same stabilizer. A massive coagulation is occurring at the largest stirring speeds, as demonstrated in Figure 4 (Table 1, entries 5 and 6, 45 and 100 rpm). In this last case, most of the polymer is a block, bulky phase, even though a few discrete particles can still be identified.

The molecular weight of the final polymer is also exhibiting important differences at different stirring speeds (Figure 5). The maximum height of each distribution is normalized for clarity; therefore, the area below each curve *does not* correspond to the actual sample conversion. From these data it is clear that the MWDs of the polymers obtained at 0, 15, 25, and 45 rpm are practically superimposed, with a weight-average molecular weight of the larger peak close to 450 kg/mol. At stirring speeds larger than 45 rpm, the MWD shifts to lower values, approaching a minimum average value of about 20 kg/mol at 400 rpm. Note that the MWD of the polymer obtained in this last case is extremely close to that of the polymer obtained without stabilizer (Table 1, entry 2).

After having examined the effect of stirring, a detailed kinetic analysis was carried out under "stable" conditions, i.e., at 25 rpm. The results are again summarized in Table 1, entries 1a−1e. Figure 6 shows the reproducibility of the experiments in terms of pressure profile as a function of time. The reasonably constant value of initial pressure (125 ± 3 bar) confirms the reliability of the CO_2 feeding system. It is worth noting that different time shifts, in the range ±0.3 h, were applied to each pressure profile in order to superimpose all of them in the region of maximum reaction rate, i.e., at the maximum slope. These shifts are needed to cancel out the different reaction induction times. Note that the experimental time values in Table 1 have been corrected accordingly. The small inset in the same figure demonstrates the time evolution of pressure and temperature

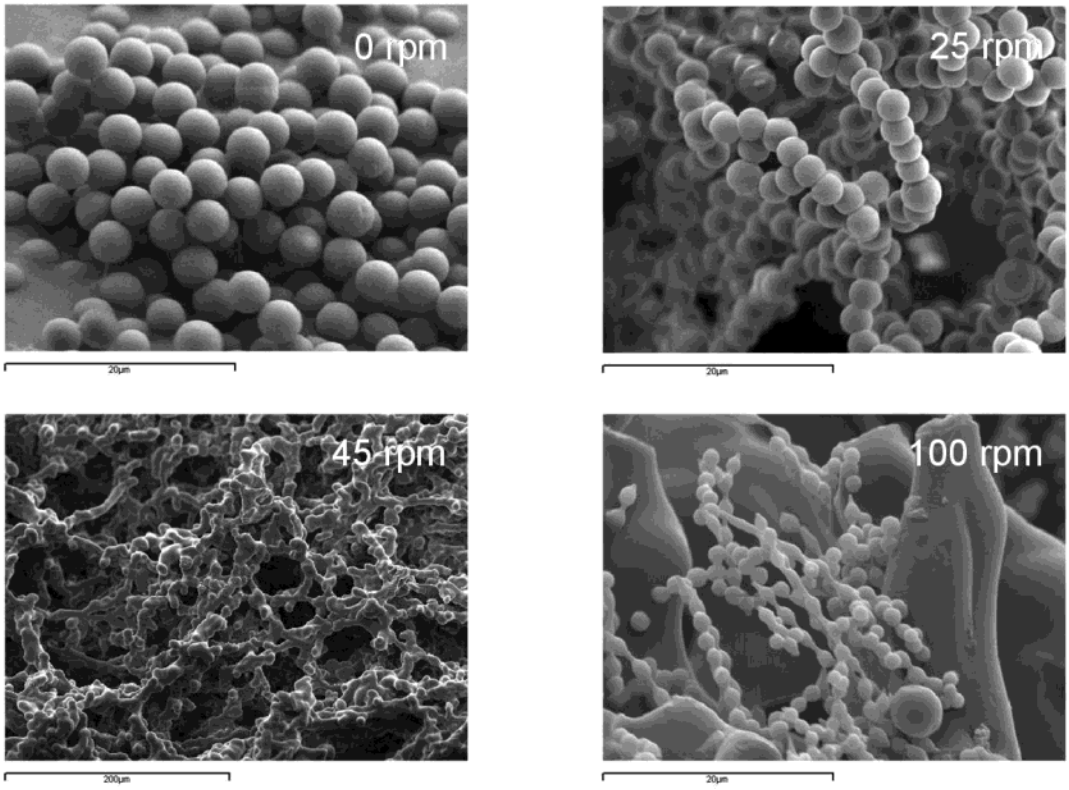

Figure 4. SEM pictures of the polymers obtained at 0, 25, 45, and 100 rpm (runs 3, 1e, 5 and 6 in Table 1, respectively).

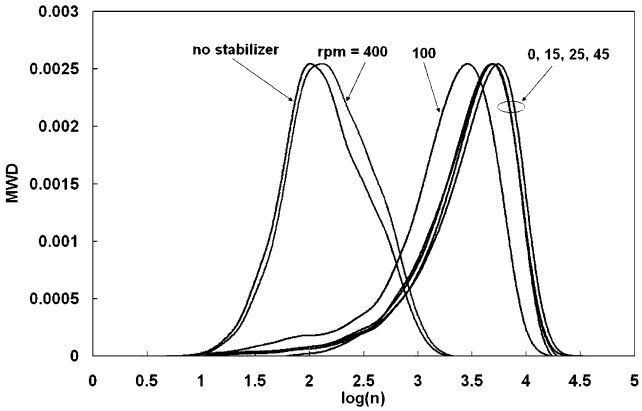

Figure 5. MWDs of the final polymer obtained at different stirring speeds. Numerical labels correspond to the stirring speed in rpm (runs 1e and 3 to 7 in Table 1); the label "no stabilizer" corresponds to run 2 in Table 1.

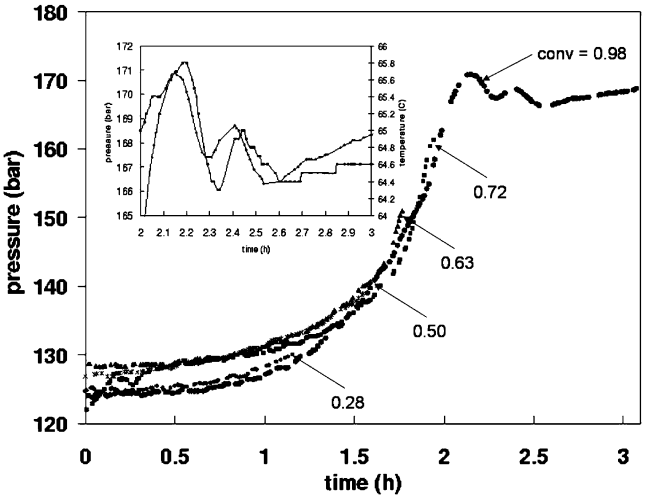

Figure 6. Pressure vs time evolution for the reactions at 25 rpm quenched at different times. Numerical labels correspond to the final conversion of runs 1a to 1e in Table 1. Inset: pressure and temperature vs time for reaction 1e (time range: 2−3 h).

during the final part of reaction 1e. By comparison of the two curves, it is evident that the oscillating behavior is the result of poor thermal control when the reaction is practically complete.

The SEM picture of the polymer at final conversion (Table, entry 1e, and Figure 4) clearly shows a particulate product, with particle diameter of approximately 2 μm matching those previously reported.[12] The particle size distribution as observed in the images appears very narrow, suggesting that the nucleation period is short and that formation of new particles by secondary nucleation is negligible.

The measured MWDs of the polymer obtained at different conversions (Table 1, entries 1a−1e) are shown in Figure 7. In this case, the area below each distribution has been normalized to the corresponding conversion, so as to facilitate comparison. The clear increase of the average molecular weight with conversion is in agreement with previous literature results[8,15] and can be attributed to the gel or Tromsdorff effect. Relatively broad distributions were found at all conversions, with polydispersity values ranging from 3.2 to 4.6 and slightly increasing with conversion. These large values can be understood by detailed inspection of the distributions in Figure 7, revealing the presence of shoulders

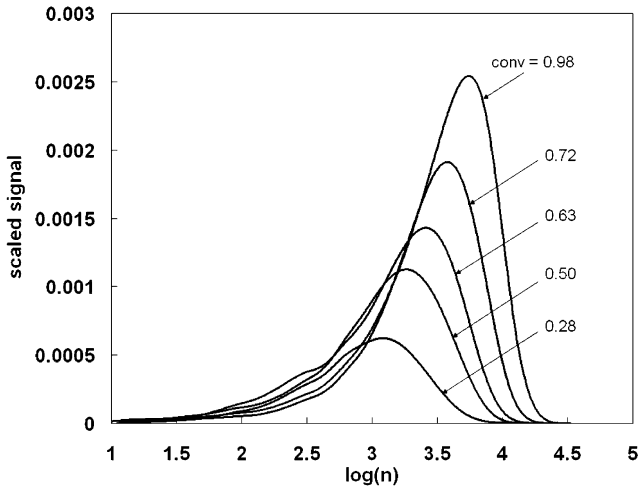

Figure 7. MWDs of the polymers obtained at different conversions at stirring speed of 25 rpm. Numerical labels correspond to the final conversion of runs 1a to 1e in Table 1.

in the low molecular weight region and at all conversion values. In contrast with the high molecular weight peaks, these low molecular weight shoulders do not exhibit any shift in molecular weight with conversion.

4. Discussion

In general, in dispersion polymerizations two polymerization loci are expected to contribute to the polymer production:[7] the CO_2-rich continuous phase and the polymer-rich dispersed phase. The mass transport of all reactants between the two phases is a key factor in determining the relative importance of each polymerization locus. Since the rate of these processes is proportional to the interphase surface, and poor stabilization of the polymer particles favors the formation of a bulky polymer phase with low interphase surface area, it follows that particle stability affects the rate of the transport processes. In particular, poor stabilization would reduce the transport of monomer and active radicals from the continuous phase, thus reducing the polymerization rate inside the particles. This is similar to the case of precipitation polymerization, where the polymer formed is segregated out of the continuous phase, and, because of the limited solubility of the monomer into the polymer phase, it is accumulated without further significant reaction.[16] At the other extreme, when conditions corresponding to good stabilization are achieved, the relative contribution of each reaction locus is determined by thermodynamic and kinetic factors (e.g., interphase partitioning and mass transport) and may change during reaction. At the beginning, the only active locus is the continuous phase, where the first polymer chains are produced. However, as soon as particles are formed, monomer, initiator, and active species are partitioned between the two phases (continuous and dispersed), and both loci are effective. Under stable conditions, the particles quickly become the dominant reaction locus because of the much slower termination rate. The initial stage of the reaction (particle formation) has been recently analyzed experimentally by Fehrenbacher and Ballauff.[17] It was convincingly shown that, if a suitable stabilizer is used, a large number of small particles are obtained in a very short time, which implies that the polymer particles become the dominant reaction locus soon after a few percent conversion.

Let us now reconsider the experimental runs at different stirring speeds shown in Figure 3. The pressure vs time curves roughly indicate the transition from stable (0−45 rpm) to intermediate (100 rpm) to completely unstable conditions (400 rpm). In the latter case, since the polymer particles coagulate, they cannot be supplied by monomer from the continuous phase, and then the reaction can proceed only in the CO_2-rich phase. However, since the pressure curves in Figure 4 show that in these conditions the polymerization rate is very low, we can conclude that the propagation reactions in the CO_2-rich phase are slower than in the polymer particles under stable conditions. The same conclusion emerges even more clearly when looking at the MWDs shown in Figure 5: while large values of the average molecular weight are achieved in stable polymer particles (order of 40 kg/mol), smaller values are obtained when faster stirring rates are applied. In particular, the same short chains are obtained when using the maximum stirring rate (400 rpm; run 7 in Table 1) and without stabilizer (run 2 in Table 1). This clearly shows that in both cases unstable, precipitation-like conditions are established and that the stabilizer is completely ineffective when the stirring speed is large enough. This picture is further confirmed by the micrographs shown in Figure 4, where the transition from a well-segregated to a bulky polymer is clearly apparent.

To support the above conclusion, it is useful to attempt a quantification of the observed destabilization process caused by stirring. Two main mechanisms are responsible for the collision of particles in the size range of relevance in this work:[18] Brownian (thermal) diffusion and convective flow due to stirring in the high pressure reactor. Sedimentation and particle breakage have been neglected because of (i) the relatively small particle size and (ii) the low stirring, respectively. The coagulation rate due to Brownian diffusion of equal size particles is given by the classical equation[19]

$$\mathscr{R}_{\text{Brownian}} = \frac{8}{3}\frac{kT}{\mu} n^2 \tag{1}$$

where k is the Boltzmann constant, T the temperature, μ the viscosity of the continuous phase, and n the particle concentration. On the other hand, to estimate the effect of stirring on the coagulation rate, it is first necessary to evaluate the fluid dynamic conditions prevailing inside the reactor. These are determined by the value of the reactor Reynolds number defined as follows:

$$Re = \frac{\rho N D^2}{\mu} \tag{2}$$

where ρ is the density of the continuous phase, N the stirring speed, and $D = 2.5$ cm the stirrer diameter. Because of the small viscosity value typical of supercritical fluids, the obtained values of Re are always larger than 1000 for all the investigated stirring speeds. This indicates that the reactor operates under transition to fully turbulent conditions.[20] Note that, in the frame of this analysis, $\mu = 5 \times 10^{-4}$ g/(cm s) and $\rho = 0.5$ g/cm^3 have been taken as representative of the fluid conditions at the adopted operating pressure and temperature.

Following the classical Kolmogoroff theory, turbulence is characterized by a cascade of eddies, where the smallest ones, which are responsible for energy dissipation, have a characteristic size given by[21]

$$\eta = \left(\frac{\mu^3}{\epsilon\rho^3}\right)^{1/4} \tag{3}$$

where ϵ is the energy dissipation rate. The average value of the dissipation rate in a stirred vessel, $\bar{\epsilon}$, can be evaluated using semiempirical relationships expressing the so-called power number, N_{Po}, as a function of the reactor Reynolds number (cf. ref 20). For the large values of Re indicated above, these relations led to

$$\bar{\epsilon} = \mathscr{C}\frac{4N^3D^5}{\pi HT^2} \tag{4}$$

where $H = 12$ cm is the estimated reactor height, $T = 8$ cm is the reactor internal diameter, and the constant $\mathscr{C}$ can be approximated to 1 in the case of unbaffled reactors with turbine impeller.[20] This leads to values of $\bar{\epsilon}$ ranging from 7.5×10^{-4} to 47.9 cm^2/s^3 as the stirring speed ranges from 20 to 400 rpm. However, a distribution of dissipation rates is typically established inside the vessel, where the largest values are typically in the region around the impeller. Computational fluid dynamics calculations carried out using commercial CFD codes[22] for the dispersing phase only (without particles), and the actual reactor geometry indicated that the maximum values of ϵ can be about 50 times larger than the estimated averages, $\bar{\epsilon}$. This means that the largest values of the energy dissipation rate in the reactor range from 3.7×10^{-2} to 2.4×10^3 cm^2/s^3, again at stirring speeds from 20 to 400 rpm. Using eq 3, this leads to values of the size of the dissipating eddies ranging from about 9 to 130 μm, depending upon the stirring rate. This indicates that the particles, whose maximum radius is of the order of 1 μm, are much smaller and, therefore, move within the eddies under shear flow conditions.

Under these conditions the coagulation rate due to stirring can be calculated using the classical relation developed by Smoluchowski (cf. ref 19):

$$\mathscr{R}_{\text{shear}} = \frac{4}{3}\dot{\gamma}(2r)^3 n^2 \tag{5}$$

where r is the particle radius and $\dot{\gamma}$ the shear rate, which, following Saffman and Turner,[23] can be computed from the maximum energy dissipation rate as follows:

$$\dot{\gamma} \simeq \left(\frac{\rho\epsilon}{\mu}\right)^{1/2} \tag{6}$$

The overall coagulation rate, $\mathscr{R}$, given by the sum of Brownian and shear contributions, is shown in Figure 8a−c as a function of the stirring speed for three values of the particle size: 0.1, 0.5, and 1 μm, being the last value that typical of stable conditions for our experiments. Note that the particle concentration n has been estimated assuming that all particles have the same size, and the overall amount of polymer is the one corresponding to full conversion. By inspection of the calculated curves, the following conclusions can be drawn:

1. Particles of different size exhibit largely different coagulation behavior, being the shear-induced contribution quite limited for the smallest particles and completely dominant for the largest ones. For the 1 μm

particles, the impact of the shear produces an acceleration with respect to the Brownian mechanism of about 100 times at around 50 rpm.

2. As mentioned above, the values of the coagulation rates shown in Figure 8a−c correspond to fully destabilized particles. In the presence of Krytox these values should be reduced by a factor equal to $1/W$, where W is the Fuchs stability ratio (cf. ref 19). The experimental data (see Figure 4) show that for particles of 1 μm the dispersion is stable in the absence of stirring while coagulation appears already at 45 rpm. In the absence of stabilization, the characteristic times for coagulation at 0 and 45 rpm can be estimated from Figure 8c as follows: $t_{\text{Brownian}} = n/\mathscr{R}_{\text{Brownian}} = 0.5$ s and $t_{\text{shear}} = n/\mathscr{R}_{\text{shear}} = 0.005$ s, respectively. If we assume that this value has to be larger than 100 s in order to have a stable dispersion but smaller than that in order to justify the occurrence of coagulation, we can conclude that the stability ratio has to fall in the interval 10^3−10^4. This is on the lower end of the values typical of stable dispersions (cf. ref 24) and confirms the weak stabilizing effect of Krytox in the system. It is worth noting that the result of this analysis is based on the values of the ratios of the coagulation rates and not on their absolute values, which are expected to be more affected by all inaccuracies inevitably present in this approximated discussion. On the basis of the above results, we can explain our experimental observations as follows.

In general, the system under examination is prone to shear-induced coagulation already at slow stirring speed, i.e., about 50 rpm. At high stirring speed (>100 rpm), a massive coagulation is taking place already at small particle size (cf. values in Table 1). Since the reaction is still proceeding and the operating temperature is larger than the glass transition temperature of the polymer (cf. ref 25), a complete interfusion of the nucleated polymer particles takes place, so that their identity cannot be recognized at the end of the reaction. Consequently, we observe the bulk morphology shown in Figure 4 at 100 rpm. In this figure it can be seen that small particles are continuously formed, but they eventually merge with the bulky polymer. Under these conditions of heavy coagulation, the interphase surface is reduced so much that the polymerization in the particle phase is significantly depressed, as confirmed by the shallow pressure−time curve in Figure 3. This also explains the observed MWD (Figure 5) which clearly demonstrates that in these conditions the polymerization proceeds mainly in the continuous phase.

At higher stirring speed, i.e., 400 rpm, coagulation is complete so that the reaction proceeds only in the CO_2-rich phase, and it becomes similar to that without stabilizer (run 2 in Table 1). Accordingly, the pressure vs time curves shown in Figure 4 and the MWDs in Figure 5 are substantially identical in the two cases. On the other hand, at lower stirring speed (25 and 45 rpm), the pearl necklace-like morphology of the particles (Figure 4) gives some significant insight into the coagulation mechanism. This morphology is in fact typical of shear-induced coagulation, as reported for example by Ali and Zollars[26] in the case of colloidal particles of polystyrene in water, and can be explained in terms of preferential orientation of the string of particles during coagulation due to the shear flow field. It is worth pointing out that pearl necklace-type aggregates can be found only when the system is not fully destabilized, as it is the case for the system under examination at moderate stirring. The difference between the morphologies obtained at 25 and 45 rpm can be explained by considering that, according to the results in Figure 8a−c, the particle size at which coagulation takes place

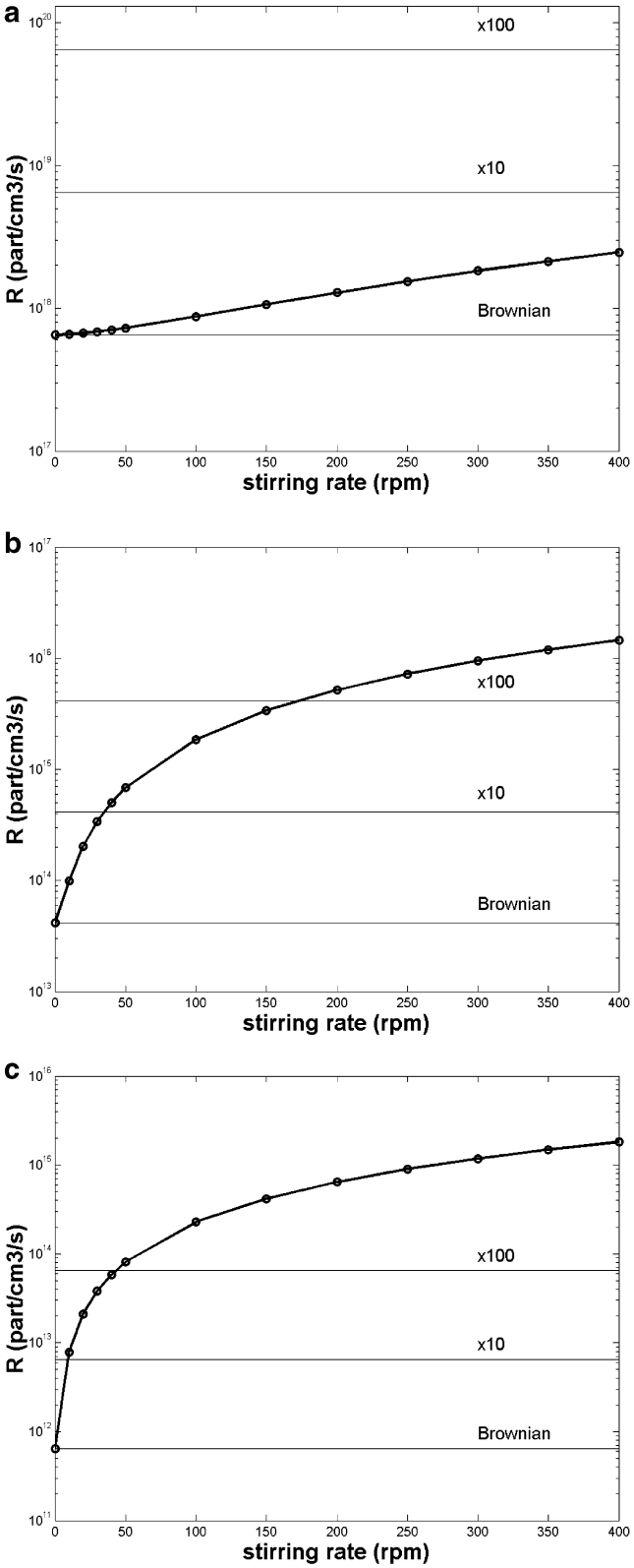

Figure 8. Calculated coagulation rate as a function of the stirring speed for three particle sizes: (a) = 0.1 μm, (b) = 0.5 μm, and (c) = 1 μm. Horizontal lines identify the Brownian coagulation rate ×1, ×10, and ×100, respectively.

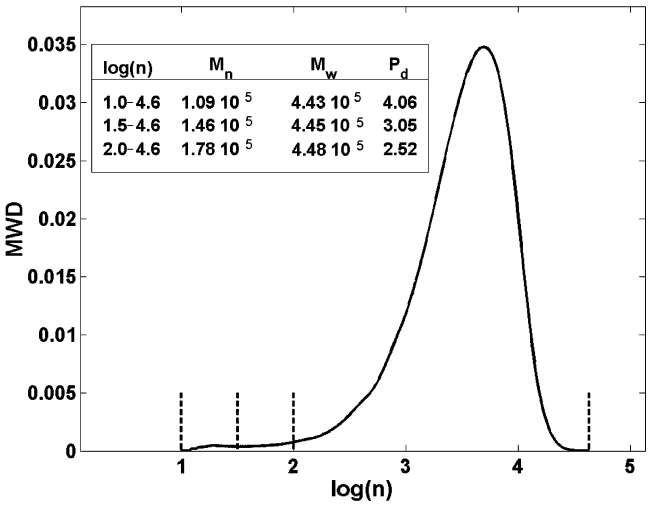

Figure 9. Role of different settings of the GPC limits log(*n*) on the calculated average molecular weights. Vertical segments indicate the considered settings.

decreases as the stirring speed increases. Therefore, at 25 rpm coagulation occurs only toward the end of the polymerization (cf. values in Table 1), so that the limited amount of monomer left to react is not sufficient to interfuse the particles with each other, and these therefore still exhibit their individual identity. On the other hand, at 45 rpm, where the same coagulation occurs at smaller particle size, and therefore at smaller conversion, the residual monomer is sufficient to produce a significant interfusion, so that the particle identity is lost. Note that in both cases particle destabilization is not sufficient to affect the reaction kinetics, as indicated by the pressure vs time curves which remain similar to that without stirring (cf. Figures 3 and 5). This means that in these cases the dominant locus of reaction are the polymer particles, and the contribution of the polymerization in the continuous phase is limited, as confirmed by the MWD in Figure 5 where the low molecular weight shoulder is much smaller than the high molecular weight main peak.

Finally, let us discuss the reaction kinetics under "stable" conditions, i.e., in the absence of stirring (runs 1a−1e in Table 1). All MWDs shown in Figure 7 exhibit a main peak and a shoulder or secondary peak at lower molecular weight values. As mentioned above, it is seen that while the high molecular weight peak moves to larger chain lengths as conversion increases, the low MW shoulder remains located roughly at the same average chain length. These different behaviors can be explained in terms of different polymerization loci. The high MW material is produced in the polymer particles where the viscosity of the medium increases due to the increase of the polymer-to-monomer ratio, which in turn leads to a decreasing termination rate constant due to increasing diffusion limitations. On the other hand, the low MW material is produced in the continuous phase, where diffusion limitations play a negligible role, and therefore the change with conversion is insignificant. This conclusion is further supported by the fact that for the polymer obtained under unstable conditions, either at high stirring rate or without stabilizer, the MWDs are in both cases monomodal (Figure 5) and centered at about the same location as the low molecular weight shoulder in Figure 7. As discussed above, this corresponds to polymer produced in the continuous phase.

It is worth noting that the polydispersity values measured under stable conditions are significantly larger than those reported in the literature for the same system under similar operating conditions.[9,11,12] Fortunately, it has been possible to reanalyze at least the samples considered in refs 11 and 12, and it was found that the discrepancy arises from the settings of the limits on the GPC curve analysis. This is clearly illustrated in Figure 9, where the inset table demonstrates the effect of the set GPC limits log(*n*) on the estimated values of M_n, M_w, and P_d. From the analysis about the two polymerization loci reported above, it is clear that the interval that includes the low molecular weight is the correct choice.

5. Conclusions

The main results of the experimental analysis of methyl methacrylate polymerization under supercritical conditions reported in this work can be summarized as follows:

1. The pseudo-graft stabilizer Krytox 157 FSL is effective and produces high yields of pure polymer under stable conditions. However, there is a strong sensitivity to mechanical stirring. The main coagulation mechanism is shear-induced, and this begins to operate at surprisingly low stirring speeds. Without stirring, the system is colloidally stable, which means that the stabilizer is effective with respect to Brownian coagulation.

2. Polymerization is taking place in two phases, continuous and dispersed, although to a different extent. Even though the polymer particles are the dominant reaction locus, where high MW material is produced, a nonnegligible amount of low MW material is produced in the continuous phase. The level of these "oligomers" is sufficient to cause a significant broadening of the final MWD, with final polydispersity values larger than those typical for the same polymer obtained in bulk or in emulsion.

The practical impact of these findings is twofold. On one hand, a careful choice of reactor geometry and stirrer type appears to be crucial when using weakly anchoring stabilizers of the type considered here. Such stabilizers are particularly attractive for high-purity applications since they are very easily removed from the polymer during the final venting phase. However, to achieve stability conditions comparable to those of typical water suspensions and emulsions, it is clear that more efficient emulsifiers have to be produced, leading to an increase of the stability ratio of about 2 orders of magnitude. On the other hand, the MWD broadening due to the polymerization in the continuous phase must be carefully considered, since the presence of low molecular weight materials and a broad MWD might have a significant impact on the end-use properties. It is important that optimized reaction conditions are identified to control this MWD broadening if these polymerization processes have to be used for industrial applications.

Acknowledgment. The financial support of EU (Project ECOPOL, Contract G1RD-CT-2002-00676) is gratefully acknowledged. M.M. thanks BBW (Swiss Federal Office for Education and Science, Contract 02-0131) for financial support. S.M.H. thanks the EPSRC for financial support and the Royal Society for a Wolfson Research Merit Award.

References and Notes

(1) Canelas, D. A.; DeSimone, J. M. *Adv. Polym. Sci.* **1997**, *133*, 103−140.
(2) Cooper, A. I. *J. Mater. Chem.* **2000**, *10*, 207−234.
(3) Lora, M.; McHugh, M. A. *Fluid Phase Equilib.* **1999**, *157*, 285−297.
(4) Wells, S. L.; DeSimone, J. M. *Angew. Chem., Int. Ed.* **2001**, *40*, 519−527.
(5) Romack, T. J.; Maury, E. E.; DeSimone, J. M. *Macromolecules* **1995**, *28*, 912−915.
(6) Saraf, M. K.; Wojcinski, L. M., III, Kennedy, K. A.; Gerard, S.; Carpentier, P. A.; DeSimone, J. M.; Roberts, G. W. *Macromol. Symp.* **2002**, *182*, 119−129.
(7) Croucher, M. D.; Winnik, M. A. In *An Introduction to Polymer Colloids*; Candau, F., Ottewill, R. H., Eds.; Kluwer Acad. Pub.: Dordrecht, 1990; pp 35−72.
(8) O'Neill, M. L.; Yates, M. Z.; Johnston, K. P.; Smith, C. D.; Wilkinson, S. P. *Macromolecules* **1998**, *31*, 2838−2847.
(9) Lepilleur, C.; Beckman, E. J. *Macromolecules* **1997**, *30*, 745−756.
(10) Sarbu, T.; Styranec, T.; Beckman, E. J. *Nature (London)* **2000**, *405*, 165−168.
(11) Christian, P.; Howdle, S. M.; Irvine, D. J. *Macromolecules* **2000**, *33*, 237−239.
(12) Christian, P.; Giles, M. R.; Griffiths, R. M. T.; Irvine, D. J.; Major, R. C.; Howdle, S. M. *Macromolecules* **2000**, *33*, 9222−9227.
(13) Christian, P.; Giles, M. R.; Howdle, S. M.; Major, R. C.; Hay, J. N. *Polymer* **2000**, *41*, 1251−1256.
(14) Thermophysical Properties of Fluid Systems, NIST Standard Reference Database No. 69, March 2003 release.
(15) Hsiao, Y. L.; Maury, E. E.; Desimone, J. M.; Mawson, S.; Johnston, K. P. *Macromolecules* **1995**, *28*, 8159−8166.
(16) Guyot, A. In *Comprehensive Polymer Science*; Alley, G., Bevington, J. C., Eds.; Pergamon Press: Oxford, 1989; Vol. 4, Chapter 16.
(17) Fehrenbacher, U.; Ballauff, M. *Macromolecules* **2002**, *35*, 3653−3661.
(18) Shaw, D. J. In *Introduction to Colloid and Surface Chemistry*, 3rd ed.; Butterworth: London, 1986.
(19) Overbeek, J. Th. In *Colloid Science*; Kruyt, H. R., Ed.; Elsevier: Amsterdam, 1952; Vol. 1, Chapter 7.
(20) Bates, R. L.; Fondy, P. L.; Fenic, J. G. In *Mixing*; Uhl, V. W., Gray, J. B., Eds.; Academic Press: London, 1966; Vol. 1, Chapter 3.
(21) Pope, S. B. In *Turbulent Flows*; Cambridge University Press: Cambridge, 2000; Chapter 6.
(22) *FLUENT 6.0 User's Guide*; Fluent Inc.: Lebanon, NH, 2001.
(23) Saffman, P. G.; Turner, J. S. *J. Fluid Mech.* **1956**, *1*, 16−30.
(24) Ottewill, R. H. In *Emulsion Polymerization and Emulsion Polymers*; Lovell, P. A., El-Aasser, M. S., Eds.; Wiley: Chichester, 1997; Chapter 3.
(25) Condo, P. D.; Johnston, K. P. *J. Polym. Sci., Part B: Polym. Phys.* **1994**, *32*, 523−533.
(26) Ali, S. I.; Zollars, R. J. *J. Colloid Interface Sci.* **1987**, *117*, 425−430.

MA030262W